PtO$_x$-SnO$_x$-TiO$_2$ catalyst system for methanol photocatalytic reforming: influence of cocatalysts on the hydrogen production

E. Tálas[1*], Z. Pászti[1], L. Korecz[1], A. Domján[2], P. Németh[1], G.P. Szíjjártó[1], J. Mihály[1], A. Tompos[1]

[1]*Institute of Materials and Environmental Chemistry, Research Centre for Natural Sciences, Hungarian Academy of Sciences, H-1117 Budapest, Magyar tudósok körútja 2, Hungary,*
[2]*NMR Research Group, Research Centre for Natural Sciences, Hungarian Academy of Sciences, H-1117 Budapest, Magyar tudósok körútja 2, Hungary*

* Corresponding author, Tel.: +36 1 382 6916, email: talas.emilia@ttk.mta.hu, address: H-1519 Budapest, P.O.Box 286, Hungary (Emília Tálas)

Abstract:

Effects of modification of PtO_x-TiO_2 photocatalysts by tin were elucidated by exploring relationships between the structural properties of variously prepared tin-loaded catalysts and their catalytic activity in methanol photocatalytic reforming. Tin free and amorphous tin-oxide decorated TiO_2 samples were prepared by sol-gel method from titanium-isopropoxide. In other approach, Sn was loaded onto the sol-gel prepared TiO_2 by impregnation followed by calcination. Pt was introduced by impregnation followed by either reduction in H_2 at 400^oC or calcination at 300^oC. TEM, XRD and Raman spectroscopic measurements proved that TiO_2 existed in the form of aggregates of polycrystalline anatase with primary particle size of 15-20 nm in each of the samples. Photocatalytic hydrogen production was influenced by the combined effect of many parameters. Both the presence of Sn and the way of Pt co-catalyst formation played important role in the activity of these photocatalysts. The Sn introduction by both sol-gel method and impregnation clearly enhanced the photocatalytic activity. ^{1}H MAS NMR measurements revealed that the Sn introduction reduced the intensity of the terminal Ti-OH groups of relatively basic character considered to be unfavorable for the photocatalytic reaction. Presence of SnO_x decreased the signal of the undesirable vacancies observed by ESR. Furthermore surface SnO_x enhanced the dispersion of Pt. The formation the Pt co-catalyst by calcination was more favorable than by H_2 treatment. In case of the calcined samples *in situ* reduction of the Pt nanoparticles at the beginning of the photocatalytic reaction was suggested to be favorable for the hydrogen production. The relatively modest photocatalytical activity obtained after high temperature H_2 treatment could be related at least two processes in this system, creation of unfavorable oxygen vacancies and appearance of SnO_x covered Pt nanoparticles formed from the air exposed alloy type Pt-Sn nanoparticles. The latter means decreased number of active sites for reduction of H^+.

Keywords: calcination; high temperature H_2 treatment; cocatalyst, XPS; ESR; ^{1}H MAS NMR

1. Introduction

Photocatalytic hydrogen production is a promising approach for transforming solar energy into chemical energy for storage [1]. Methanol which can be obtained from both fossil resources and biomass [2] is an appropriate starting compound for H_2 generation due to its high H/C ratio. Many efforts have been made for efficient photoinduced reforming of methanol on semiconductive oxides in the presence of water providing H_2 and CO_2 [3-6]:

$$CH_3OH \quad + \quad H_2O \quad \underset{}{\overset{\text{Photocatalyst, h}\nu}{\rightleftharpoons}} \quad CO_2 \quad + \quad 3\ H_2 \tag{1}$$
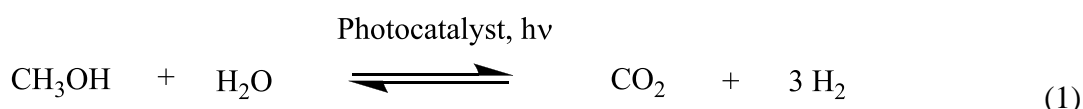
Because of its efficiency, long term stability, cheapness and low toxicity, TiO_2 is one of the most frequently used photocatalysts [7-9]. Different types of sol-gel methods are widely applied for preparation of TiO_2 [10]. Benefits derived from preparing TiO_2 by sol–gel method include the synthesis of nanosized crystallized powder of high purity at relatively low temperature, resulting in homogeneity of the prepared materials. Sol-gel methods gives possibility to introduce doping elements [11-14] or their combination simultaneously [15], to prepare composite type TiO_2-based materials [16,17]. Sol-gel method is a possible way to obtain coatings or nanocoatings [18], porous films [19] or ordered mesoporous structures [20,21].

The activity of TiO_2 in reaction (1) can be increased at least an order of magnitude when a proper cocatalyst is involved [3,22,23]. The advantages of the cocatalysts are attributed to the reduced charge recombination; promoted charge separation and transport driven by junctions/interfaces [24,25]. Another important role of the cocatalyst is to provide reaction sites for elementary reaction steps subsequent to light absorption, such as formation of molecular hydrogen and its desorption from the surface [24,25]. If the surface reaction is too slow to consume the charges, the probability of charge recombination increases. Pt is a very effective cocatalyst for H_2 production [3,25] as it shows the lowest activation energy for H_2 evolution [25,26].

In order to load metal nanoparticles on the surface of the semiconductors several different methods are available. Commonly used techniques include *in situ* photodeposition [27,28] and deposition of pre-prepared metal colloids [29,30]. Traditional way for preparing supported metal nanoparticles is impregnation with the appropriate metal salt followed by high temperature hydrogenation [31]. Calcination of the metal salt loaded on semiconductors by impregnation also resulted in effective cocatalysts for photocatalytic H_2 production [32].

In our previous work sol-gel synthesis carried out in the presence of tin compounds under relative mild conditions (*i.e.* temperature of calcination: 400°C) was used for preparation of TiO$_2$ based photocatalysts [33]. Our TEM and SEM measurements indicated the presence of micron sized aggregates built from polycrystalline anatase in those samples. XRD and Raman spectroscopic measurements proved the formation of pure anatase by our method. No evidence for tin incorporation into the lattice of TiO$_2$ was found by the above characterization methods. Nevertheless band broadening in Raman spectra and surface enrichment in Sn detected by XPS suggested that TiO$_2$ decorated with amorphous tin-oxide islands was obtained [33]. This type of tin-oxide together with metallic Pt nanoparticles formed by high temperature hydrogen treatment as a cocatalyst system considerably improved the photocatalytic activity of TiO$_2$ in the methanol photocatalytic reforming reaction [33]. Although supported Sn-Pt bimetallic catalyst are widely studied and used in various fields, there are relatively few reports dedicated to the characterization of the cocatalysts in the PtO$_x$-SnO$_x$-TiO$_2$ photocatalytic system up to now [34-36]. To the best of our knowledge no systematic study of the effect of cocatalyst formation in these systems exists; only influence of redox-treatment on Pt/TiO$_2$ system has been described [37]. Reviewing the literature on Pt/TiO$_2$ systems with Pt cocatalyst loaded by different way, certain indication can be found that the ionic state of the Pt is favorable for the photocatalytic reaction [38-40].

In this work a detailed study of the influence of the way of cocatalyst formation (hydrogen treatment *vs*. calcination after the impregnation of sol-gel TiO$_2$ with platinum salt) is given. The focus is laid on the state of platinum and tin in the cocatalyst as well as the cocatalyst-TiO$_2$ interaction. We try to find relationships between the catalytic activity observed in methanol photocatalytic reforming and the structural properties of the sol-gel TiO$_2$ loaded with platinum and tin containing cocatalyst. In order to obtain more realistic picture about the real working catalyst, results of characterization of fresh and recovered samples are compared.

2. Material and methods

2.1 Materials

Titanium-isopropoxide (≥97.0% % Sigma Aldrich) was used for the synthesis of titania nanoparticles. SnCl$_4$·5H$_2$O (Riedel-de Haen) was used as tin precursor. Citric acid used for gel formation was purchased from Sigma Aldrich. Pt(NH$_3$)$_4$(NO$_3$)$_2$ (Aldrich) was used as a

precursor of supported Pt nano-particles. Methanol, absolute ethanol solvent and hydrochloric acid (37 w %) and nitric acid (65 w %) were products of Reanal (Hungary).

2.2 Synthesis of photocatalysts

Tin free (no-Sn) and tin modified (SnOx-SG) TiO_2 samples were prepared by sol-gel method as described before [33]. Briefly, in the presence of citric acid and absolute ethanol titanium-isopropoxide was stirred for 180 min at room temperature and then heated at 65^oC until gel formation. In case of tin modified samples $SnCl_4x5H_2O$ was also introduced into the mixture at Sn/Ti ratio of 0.007. The gel was dried and calcined for 5 hours at 400^oC; the choice of the calcination temperature was restricted to relatively low values as we wanted to ensure the formation of the pure anatase phase in order to make easier the interpretation of the catalytic behavior of our system. In another approach, Sn was loaded onto the sol-gel prepared TiO_2 by incipient wetness impregnation with $SnCl_4x5H_2O$ solution followed by calcination at 300^oC (SnOx-I). The Sn load was 1 w% in both case. Pt was introduced from aqueous solution of $Pt(NH_3)_4(NO_3)_2$ by incipient wetness impregnation. Contrary to our previous work [33] the Pt load was increased to 1% which allowed the photoelectron spectroscopic (XPS) analysis of the supported platinum. The dried samples were either reduced for 1 hour at 400^oC in H_2 atmosphere or calcined for 1 hour at 300^oC. The sequence of the introduction of Sn and Pt was also varied. The lineage of the various Sn-Pt/TiO_2 catalysts is depicted in Figure 1.

Insert Figure 1

2.3 Characterization of photocatalysts

Nitrogen adsorption isotherms have been measured in volumetric equipment (ASDI RXM 100, Advanced Scientific Design Inc.) in order to determine BET specific surfaces. Samples were pretreated in inert gas flow at 200^oC for 1.5 h then evacuated and cooled to the temperature of liquid nitrogen.

Raman spectra were recorded with a dynamically aligned Bio-Rad (Digilab) dedicated FT-Raman spectrometer equipped with a Spectra-Physics Nd-YAG-laser (1064 nm) and high sensitivity liquid-N_2 cooled Ge detector. The laser power used was about 250 mW at the samples. The resolution of the Raman instrument was ca. 4 cm^{-1} and a backscattered geometry was used. For each spectrum 256 individual spectra were averaged.

Diffuse reflectance UV-visible spectra of the samples were registered using a Jasco V-570 UV-VIS spectrophotometer equipped with NV-470 type integrating sphere. The data were collected between 800 and 200 nm wavelengths with 100 nm/min speed

The solid state magic angle spinning (MAS) ^{1}H spectra of the samples were recorded on a Varian NMR System (Varian Inc., Palo Alto, CA, U.S.A.) operating at ^{1}H frequency of 400 MHz with a Chemagnetics T3 4.0 mm narrow bore double resonance probe. The ^{1}H direct polarization spectra were measured with a rotor spinning rate of 12 kHz. The [1]H $\pi/2$ pulse was 3 μs and 5 seconds of repetition delay of was used. The measuring temperature was 20°C. Spectra were recorded before and after evacuation of the samples in a vacuum oven at 130 ^{o}C for 6 hours.

The ESR experiments were performed with a Bruker Elexsys E500 X-band spectrometer. A typical microwave power of 1 mW and 1 G magnetic field modulation at ambient temperature were used. The magnetic field was calibrated with an NMR field meter. Signal intensity, linewidth and g-factor (spectroscopic splitting factor) values were used to characterize the samples. The knowledge of the g-factor can give information about a paramagnetic center's electronic structure.

X-ray photoelectron spectroscopy (XPS) measurements were carried out using an EA125 electron spectrometer manufactured by OMICRON Nanotechnology GmbH (Germany). The photoelectrons were excited by both MgKα (1253.6 eV) and AlKα (1486.6 eV) radiation. Spectra were recorded in the Constant Analyzer Energy mode of the energy analyser with 30 eV pass energy resulting in a spectral resolution around 1 eV. For XPS experiments the samples in the form of fine powder were suspended in isopropanol. Drops of this suspension were placed on standard OMICRON sample plates; after evaporation of the solvent catalyst coatings with sufficient adhesion and electric conductivity were obtained. Effects of possible electric charging were compensated by adjusting the binding energy of the main component of the C 1s envelope (hydrocarbons) to 285.0 eV. By this choice both the Ti $2p_{3/2}$ and the O 1s binding energies coincided with the range expected for TiO_2, confirming the reliability of the calibration. Chemical states of the elements were deduced from high resolution spectra using XPS databases [41,42]. Quantification was performed using combination of CasaXPS [43] and XPSMultiQuant [44,45].

2.4 Photocatalytic hydrogen generation

Catalytic reaction over different catalysts was studied in standardized reaction conditions, so that the catalytic activity of the different catalyst could realistically be compared. The photocatalytic reaction was carried out in liquid phase in a reactor system of 10 quartz glass units equipped with magnetic stirrers, gas inputs and outputs as described before [33]. The size of the cylindrical glass units were: 60 mm in height and 140 mm in

The initial concentration of methanol was 6 v % in distilled water. It has been known that the rate of hydrogen generation *vs*. methanol concentration relationship gives a saturation curve and use of diluted solution is favorable [3]. The reaction was carried out at room temperature. The amount of catalyst and the reaction volume in every unit was 0.140 g and 280 ml, respectively. Osram HQL de luxe 125W lamps were used as light sources operated in UV -visible region. Hydrogen formation was followed by GC analysis of the outlet gas upon using SUPELCO Carboxen 1010 column, TCD and FID detection and argon internal standard. After the photocatalytic reaction, the samples were recovered from the aqueous methanol solution by centrifuging, washing with 3x50 ml absolute ethanol followed by drying under N_2 flow.

3. Results and discussion

3.1 Preliminary characterization of the photocatalysts

The BET specific surfaces of the sol-gel TiO_2 samples with tin (SnOx-SG) or without tin (no-Sn) was about 60 ± 10 m^2g^{-1}. The cocatalyst formation both by calcination and impregnation reduced the specific surface area of all the samples by at about 5-15% but it was still comparable with that of Degussa P25 (47 m^2g^{-1}); one of the most popular commercial photocatalyst. The average particle size obtained for XRD measurements was about 20 nm in case of both tin containing (SnOx-SG) and tin free (no-Sn) sol-gel TiO_2. This value was confirmed by TEM images (Figure S1 in supplementary materials). The Raman spectra of the different samples were very similar to each other (see Figure 2). The results of Raman spectroscopic measurements in accordance with that of XRD measurements (Figure S2 in the supplementary materials and Figure 3 in Ref. [33]) showed that separate SnO_2 phase (with weak band in the Raman spectra at 629 cm^{-1}) did not occur in the tin containing samples. TiO_2 of rutile type (medium intensity bands at 609 and 446 cm^{-1}) cannot be detected in any samples; formation of anatase phase exclusively was proved both by Raman spectroscopy (Figure 2) and XRD (Figure S2 in the supplementary materials) in accordance with our previous finding [33]. Neither introduction of Pt nor formation of cocatalyst by hydrogenation [33] or by calcination (*cf*. lines a and b; lines d and e in Figure 2) led to the appearance of rutile phase although certain literature indication exists that reduced form of Pt can contribute

to the increase of the ratio of rutile/anatase phase in Degussa P25 [37]. Only a slight red shift and band broadening suggested an interaction between TiO_2 and oxidized Pt in case of sample SnOx-I Pt calc (spectrum e in Figure 2).

Insert Figure 2

3.2 Photocatalytic hydrogen generation

The photocatalytic H_2 production over the sol-gel prepared TiO_2 samples was almost negligible in the absence of platinum (0.03 and 0.04 $mmolg_{cat}^{-1}h^{-1}$ over no-Sn and SnOx-SG, respectively). The activity of tin containing and tin free samples decorated by different types of Pt co-catalysts was larger at least one order of magnitude (see Figure 3). Sn introduction by both the sol-gel method and impregnation clearly enhanced the activity. Surprisingly, Pt co-catalyst formation by calcination (Pt Calc) was more favorable than by H_2 treatment (Pt H2 red). It can also be seen that the improving effect of Sn was more pronounced at the calcined samples than at the hydrogenated ones.

Insert Figure 3

When the sample (no-Sn Pt H2 red) was further modified by tin using incipient wetness impregnation with $SnCl_4x5H_2O$ followed by H_2 treatment at 400°C, no activity growth was found comparing to the Sn free sample (1.07 $mmolg_{cat}^{-1}h^{-1}$ vs. 1.06 $mmolg_{cat}^{-1}h^{-1}$).

Results presented in Figure 3 generate two main questions to which answers must be given in order to understand the behavior the PtO_x-SnO_x-TiO_2 catalysts system. One of them: "What was improved by the tin?" The other one: "What was improved by the calcination?" Several possible answers could be considered: (i) the type and/or the number of the surface OH groups were influenced; (ii) the structure of the semiconductor was changed; (iii) element ratios and oxidation state of the surface elements were changed. All of these ideas are supported by literary analogies. It has already been described that the decrease in the surface OH groups of basic character was favorable in photocatalytic oxidation reactions over TiO_2 [46,47]. It has also been reported that certain vacancies could be stabilized by Pt^{n+} [48]. It could be assumed that calcination changed the surface of the semiconductor, reduced the number of recombination centers and/or promoted the surface charge transfer. The coexistence of metallic Pt and-PtO_x, which may be the result of the calcination, could also be supposed, as dual cocatalyst *i.e.* presence of metal and metal oxide together was found to be advantageous [49]. In order to obtain evidences ^{1}H MAS NMR measurements were applied to get information about the OH structure of TiO_2, while the electronic structure of the samples was characterized by ESR as well as diffuse reflectance UV-Vis spectroscopy.

Beside these methods a detailed study of the surface of fresh and recovered samples were carried out by XPS.

3.3 Results of ^{1}H MAS NMR measurements

Figure 4 shows the ^{1}H MAS NMR spectra of the Sn free (no-Sn) and Sn-modified TiO_2 samples (SnOx-SG, SnOx-I).

Insert Figure 4

In accordance with results of Jiang and coworkers [46], appearance of two distinct groups of signals could be observed; a small intensity one at low- and a larger one at high chemical shift, which belonged to the OH groups of a TiO_2. It is known that Ti-OH groups at low chemical shift are considered as terminal ones (see Figure 5A) with relative basic character [46,50] while Ti-OH groups at higher chemical shift are considered as bridging ones (see Figure 5B) with relative acidic character [46,50,51]. Adsorbed water can also give a signal in ^{1}H MAS NMR spectra of TiO_2 in the region of bridging OH [52]. According to works of Nosaka et al. the adsorbed water exists in three layers: (i) the outermost layer with highly mobile water molecules; (ii) the intermediate layer with relatively mobile water molecules; (iii) the innermost layer with rigid, barley mobile water molecules and/or hydroxyl groups [52,53]. It has been suggested that photodecomposition of ethanol should proceed in physisorbed water layers [54].

Figure 4 clearly shows that Sn introduction reduced the intensity of the terminal Ti-OH groups. In accordance with the idea of Jiang and coworkers in Ref. [46] we supposed that the decrease in the Ti-OH groups of relatively basic character could be related to the positive effect of Sn on the photocatalytic reaction. As the Sn/Ti ratio was very small in our samples (note that the Sn content was 1 w %), signals obtained from the probable formed Sn-OH groups could not be distinguished (^{119}Sn NMR measurements are targeted in our future plans).

Insert Figure 5

As emerges from Figure 4 the intensities of the signals at high chemical shift were almost the same in spectra of the three different samples. Taking into account that the BET surface areas of our samples were very close to each other, the above finding was in accordance with that of Nosaka and coworkers [52]. They reported that the amount of adsorbed water per unit surface area was almost the same for six TiO_2 samples of different type. We could deconvolute the signals at higher chemical shift at least into two signals with chemical shifts of 5.0 and 6.5 ppm. ^{1}H MAS NMR spectra recorded after evacuation of our samples at 130°C for 6 h showed certain changes. The intensity in the region of bridging OH

decreased by 10-15%. The component at higher chemical shift moved to somewhat (0.7-0.8 ppm) lower value. The component at lower chemical shift at 5.0 ppm completely disappeared which indicated the removal of the loosely bonded H-bridge structures. Nevertheless Sn free and Sn modified TiO_2 samples showed very similar changes in the region of higher chemical shifts.

3.4 Results of ESR measurements

Results of ESR measurements of Pt-free-, Pt-containing fresh and Pt-containing recovered samples are given in Figure 6. Although characteristic differences between the spectra of the samples with cocatalyst formed by hydrogenation (Figure 6A) and calcination (Figure 6B) appeared, the spectra of recovered catalysts were very similar in both cases (cf. line c in Figure 6A and line c in Figure 6B). The most noticeable difference between the spectra of this two recovered samples was the intensity of a narrow signal with g= 2.002-2.003. This signal was observed in all samples independently the presence of any form of Sn (Figure S3 in supplementary materials). The intensity of this signal was significantly increased by the Pt introduction (cf. lines a and b both in Figure 6A and Figure 6B) regardless of the presence of Sn as can be seen in Figure S3 in supplementary materials. The intensity change generated by the Pt introduction was much higher in case of the hydrogen treated samples than the calcinated ones (*cf*. line b in Figure 6A and line b in Figure 6B). According to the literature the above signal could be attributed to O^{-} anion radical [55]. At this moment we don't have enough information to describe the nature of these vacancies precisely.

In accordance with our previous findings [33], Ti^{3+} ($g_{\parallel}$=1.944, $g_{\perp}$=1.989) [56] could not be observed either in the calcined or in the hydrogenated samples. However, the *in situ* formation of Ti^{3+} under the photocatalytic reaction followed its reoxidation cannot be excluded. It should be noted that Dal Santo and coworkers [48] were able to observe Ti^{3+} but only after *in situ* irradiation experiments.

Comparing to ESR spectra obtained over fresh and recovered catalysts (*cf*. line b and c in Figure 6AB) it can be noticed that the intensity of the vacancies generated by the introduction of Pt decreased during the photocatalytic reaction.

Insert Figure 6

In order to find correlation between the photocatalytic activity and the appearance of this type of vacancies, the amounts of the produced hydrogen were depicted as a function of the signal intensities of the Pt increased vacancies of the recovered catalysts (Figure 7).

Insert Figure 7

Two linear dependencies of negative slope could be separated, a more steep one in case of the samples with cocatalyst formed by calcination and a much less pronounced one in case of the samples with cocatalyst formed by the hydrogen treatment. The appearance of two types of dependencies suggested that more than one parameter influenced the photocatalytic hydrogen production. In both series of catalysts the lowest hydrogen production belongs to the highest intensity of the new vacancies, *i.e.* the negative slopes let us to conclude that the presence of these new type of vacancies are not favorable for the photocatalytic reaction. The presence of SnO_x could contribute to the decrease of the intensity of the undesirable vacancies.

3.5 Results of diffuse reflectance UV-Vis spectroscopic measurements

Data presented in Figure 8A shows that tin introduction either by sol-gel method or impregnation did not influence the adsorption edge of TiO_2 significantly compared to the bare sol-gel TiO_2 (*cf.* line a b, c in Figure 8A). Independently of the presence of tin, the band gaps calculated from the Kubelka- Munk functions obtained from these data were about 3.1 eV which is characteristic for anatase TiO_2. Pt cocatalyst formation by hydrogenation led to totally different UV-Vis spectra according to the darkening caused by the metal nanoparticles (*cf.* line a and b, c in Figure 8B). No real change could be observed comparing the fresh and recovered catalyst if the cocatalyst was formed by hydrogenation. When the cocatalyst was formed by calcination the fresh sample less differed from Pt free TiO_2 or SnO_x-TiO_2 but the recovered catalyst showed a pronounced darkening. This observation indicated a possible *in situ* reduction of the platinum during the photocatalytic reaction. Darkening in the recovered calcined samples, consequently the *in situ* reduction of the platinum containing nanoparticles was independent from the presence of tin as diffuse reflectance UV-Vis behavior of the samples obtained from sol-gel TiO_2 named no-Sn and SnOx-I (Figure S4 in supplementary materials) was very similar.

Insert Figure 8

3.6 Results of XPS measurements

We studied the oxidation state of Pt in the fresh and recovered samples with cocatalyst formed by calcination (Figure 9) and high temperature hydrogen treatment (Figure 10). In case of the fresh catalysts obtained by calcination, mainly Pt^{2+} and Pt^0 could be detected independently of the presence of tin (*cf.* lines "after calcination" in Figure 9ABC). After the photocatalytic reaction over the calcined samples the significant part of the platinum existed

11

in the form of Pt^0 (see lines "recovered" in Figure 9ABC) as it was predicted by the UV-Vis spectra. Although, we were not able to distinguish the part of Pt-oxide obtained from reoxidation of Pt^0 during the handling of the recovered samples and the part of Pt-oxide remained unreduced during the photocatalytic reaction, the highly enhanced ratio of Pt^0 in the recovered samples compared to the freshly calcined ones in all three cases gave strong evidence for the *in situ* reduction of Pt^{+n} during the photocatalytic reaction. The possible reasons of the *in situ* formation of metallic platinum under the methanol photocatalytic reaction could be (i) reduction by the methanol and/or the product *i.e.* the *in situ* formed hydrogen.; (ii) the effect of the irradiation. Contrary to calcination, cocatalyst formation by hydrogenation resulted in almost exclusive appearance of Pt^0 already in the fresh samples (see lines "after reduction" in Figure 10ABC). In case of these samples a little change in the oxidation state of Pt was observed after the photocatalytic reaction, as expected. However it could be assumed that SnO_x capping layer provided some protection against the further oxidation of Pt. This idea was supported by the observation that the ratio of Pt^0 was only 88% in the reduced Sn-free sample (no-Sn Pt H2 red) while that was 100% in the Sn-containing ones (SnOx-I Pt H2; SnOx-SG Pt H2 red). Furthermore the ratio of Pt^0 was even lower (84%) in the recovered Sn-free sample (no-Sn Pt H2 red recovered) which was exposed to long lasting stirring in aqueous solution during the photocatalytic reaction. ~~Taking~~ Nevertheless, taking into account that the photocatalytic activity of all the calcined samples was higher than that of the corresponding hydrogenated samples, it could be concluded that the *in situ* formation of Pt nanoparticle is favorable for the photocatalytic reaction. However Pt spectra did not provide enough evidence for the positive effect of the coexistence of zero valent state and oxidized form (dual cocatalyst) as the recovered samples with the lowest and the highest activity in the photocatalytic hydrogen production both contained Pt in ionic form.

Insert Figure 9

Insert Figure 10

In the tin-containing samples Sn existed in oxidized form (SnO_2) even in the H2 red series of the catalysts (see line "as prepared" in Figure 11). The binding energy of the Sn $3d_{5/2}$ peak was somewhat lower than that expected for SnO_2, but the Sn $M_4N_{45}N_{45}$ Auger peak was sharp and the Auger parameter (919.0 eV) corresponded to the Sn^{4+} ionic state. Note that all catalysts were exposed to air during the sample preparation for XPS. In order to make the picture complete, *in situ* hydrogen treatment (in the preparation chamber of the photoelectron spectrometer) was also applied. After this *in situ* reduction contribution from metallic Sn clearly appeared in both the Sn 3d spectrum and the Sn MNN Auger spectrum (see line

"200°C 60 min reduced" in Figure 11). The very low binding energy of the Sn 3d$_{5/2}$ peak indicated electron rich environment, while the value of Auger parameter was 921.6 eV which significantly differed from that of bulk metallic Sn (922.4 eV), and is interpreted as the sign of the formation of a Sn-Pt alloy phase.

Insert Figure 11

It is known that Sn can be reduced easily only in the very near neighborhood of Pt, during which formation of Sn-Pt alloys may take place [57,58]. The ratio of the surface metallic Sn to surface total Sn content after the *in situ* reduction was in the range of 19-25 % in every Sn containing sample of this work. Consequently, we believe that a certain part of Sn was in close proximity to Pt in our samples, independently the way of tin introduction.

Based on quantitative evaluation of the data from the XPS measurements of fresh and recovered catalysts, surface Pt/Ti and Sn/Ti ratios were calculated and correlated with the photocatalytic hydrogen production (Figure 12).

Insert Figure 12

Figure 12 clearly shows that the samples with different cocatalyst activation routes followed different tendencies. When the cocatalyst was formed by calcination, the Pt/Ti ratios increased with the increasing tin content. As the amount of introduced Pt was equal in all these samples and Pt contents measured by ICP after dissolution in aqua regia were equal within the margin of error, the alteration in surface Pt/Ti ratio likely to be connected to the increase in the dispersion of the Pt [59]. Influence of the Sn introduction on size of the Pt nanoparticles was also indicated by TEM images of the samples (see Figure S5-S8 in the supplementary material). In the series of calcined samples Pt/Ti ratios were lower in the recovered catalysts than in the fresh ones, which indicated certain stability problems. The hydrogen production increased with the increasing Pt/Ti ratio and the presence of tin had positive effect on the activity. On the contrary, when the cocatalyst was formed by high temperature hydrogen treatment, the Pt/Ti ratios depended on the tin content scarcely. The Pt/Ti ratio in the hydrogenated samples was almost always lower than that in the calcined samples. This observation could be explained by the lower dispersion of Pt and/or the possible decoration of the supported metal with TiO$_x$ which is known in the literature [60]. In case of the cocatalyst obtained by high temperature hydrogen treatment no significant change in the Pt/Ti ratio was induced by the photocatalytic reaction so these systems seemed more stable than the calcined ones. The presence of tin also increased the activity to a certain limit as we described before [33].

Comparing the Sn/Ti ratio in the fresh catalysts with different way of Sn introduction (SnOx-SG Pt Calc=0.011; SnOx-SG H2 red =0.012; SnOx-I Pt Calc=0.104; SnOx-I H2 red= 0.079), it can be seen that the surface Sn contents were much lower when the Sn was introduced by sol-gel method than done by impregnation. It is obvious, because the Sn covered nanoparticles existed in aggregated form in the samples obtained by sol-gel type Sn introduction which partially hid the Sn. Conversely, only the outer surface of the aggregated nanoparticles was available for the tin solution in case of impregnation type Sn introduction. In the case of the calcined catalysts, the outstanding Pt/Ti ratio both in the fresh and the recovered sample (0.029, 0.020 respectively) connected with the highest photocatalytic activity was obtained in the presence of Sn introduced by impregnation (SnOx-I Pt Calc). It is known that Sn^{n+} on the surface can promote the stabilization of Pt [61]. In contrast, the high temperature hydrogen treated counterpart (SnOx-I Pt H2 red) gave the lowest Pt/Ti ratio both in fresh and recovered samples (0.007, 0.009 respectively). The *in situ* H_2 treatment of the samples at $200^{o}C$ before recording XPS spectra gave surprising results: 2-3-fold increase of Pt/Ti ratio in the fresh and recovered SnOx-I Pt H2 red samples and no significant change of Pt/Ti ratio in other samples were observed. In the same time the Sn/Ti ratio decreased in the fresh and recovered SnOx-I Pt H2 red samples. These observations make it unlikely that TiO_2 climbed on the top of the emerging metal nanoparticles during the high temperature reduction of the metal precursor. On the contrary, it seems reasonable to assume that Pt particles in this sample became covered by a thin coating during the reductive activation, which was removed by the *in situ* reduction at relative mild conditions. This thin coating is supposed to be tin-oxide. As we mentioned above, SnO_x can only be reduced at relative mild conditions if it is in intimate contact with Pt [57,58] thus we suppose that some part of the Pt containing nanoparticles was covered by SnO_x in the sample SnOx-I Pt H2 red (and in the used one). Our *in situ* reduction experiments suggested Sn-Pt alloy formation even in the case of the calcined SnOx-I Pt samples, while it is well established that oxidation of Sn-Pt alloys results in extensive segregation of tin oxide onto the surface [62] especially in nanosized systems [63]. Thus the thin SnO_x on the top of Pt-containing nanoparticles could form easily and quickly via migration of tin to the surface and stabilization there in the form of tin-oxide [57,58] when supported Sn-Pt alloy nanoparticles are exposed to air during the handling. When the surface concentration of Sn is high enough and the cocatalyst is formed by high temperature hydrogen treatment, the amount of the formed Sn-Pt alloy can be significant. Alloy formation in the calcined samples is not possible during the reduction of photocatalytic reaction at room temperature.

Regarding the SMSI, we examined the surface Pt/Ti ratios calculated from XPS data in the Sn–free samples where the presence of capping SnO_x layer did not disturb. Comparing surface Pt/Ti ratios in samples with cocatalyst formation by calcination to surface Pt/Ti ratios in samples with cocatalyst formation by high temperature hydrogen treatment in as received form and after *in situ* hydrogen treatment, these values were almost identical within the margin of error. (Table S2 in the supplementary material). This observation let us to conclude that even if SMSI appears, its extent is more or less equal in the calcined and the high temperature hydrogen treated samples.

A simplified scheme of the assumed transformations of the supported nanoparticles prepared by different cocatalyst formation is presented in Figure 13. Regarding the role of the thin SnO_x lining on the top the Pt nanoparticle in the photocatalytic hydrogen production, it could decrease the number of active sites for reduction of H^+ significantly; consequently it could lead to decreased activity in H_2 production.

Insert Figure 13

4. Conclusions

Photocatalytic hydrogen production in methanol photocatalytic reforming over PtO_x-SnO_x-TiO_2 catalysts system is influenced by combined effect of many parameters. Both the presence of Sn and the way of Pt co-catalyst formation play important role in the activity of this type of photocatalysts. The following benefits of Sn introduction can be suggested: it can decrease the number of the unfavorable, relatively basic type of OH groups and the intensity of the undesirable vacancies. Furthermore it can provide a relatively high dispersion of Pt. As far as cocatalyst formation is concerned, our studies revealed that activation by high temperature hydrogenation has clear negative effects, which can be related to at least two processes in this system: creation of unfavorable oxygen vacancies and appearance of SnO_x covered Pt nanoparticles formed during air exposure of alloy type Pt-Sn nanoparticles. The latter means decreased number of active sites for reduction of H^+. On the contrary, cocatalyst formation by calcination not only avoids these problems, but provides beneficial Pt-PtO_x interfaces also. It can be concluded that Pt cocatalyst is important not only as an electron sink which helps to prevent the charge recombination but also as a catalytic active site in the PtO_x-SnO_x-TiO_2 photocatalyst system.

References

[1] L.P. Bicelli, Int. J. Hydr. Energy 11 (1986) 555–565.

[2] C.N. Hamelinck, A.P.C Faaij, J. Power Sources 111 (2002) 1-22.

[3] L.S. Al-Mazroai, M. Bowker, P. Davies, A. Dickinson, J. Greaves, D. James, L. Millard, Catal. Today 122 (2007) 46–50.

[4] G. Wu, T. Chen, X. Zong, H. Yan, G. Ma, X. Wang, Q. Xu, D. Wang, Z. Lei, C. Li, J. Catal. 253 (2008) 225–227.

[5] G.L. Chiarello, M.H. Aguirre, E. Selli, J. Catal. 273 (2010) 182–190.

[6] T.A. Kandiel, R. Dillert, L. Robben, D.W. Bahnemann, Catal. Today 161 (2011) 196–201.

[7] X. Chen, S.S. Mao, Chem. Rev. 107 (2007) 2891-2959.

[8] M. Ni, M.K.H. Leung, D.Y.C. Leung, K. Sumathy, Renew. Sust. Energ. Rev. 11 (2007) 401–425.

[9] A. Fujishima, X. Zhang, D.A. Tryk, Surf. Sci. Rep. 36 (2008) 515–582.

[10] U.G. Akpan, B.H. Hameed, Appl. Catal. A: General 375 (2010) 1–11 and the references cited herein.

[11] X. Qiu, C. Burda, Chem. Phys. 339 (2007) 1–10.

[12] H. Sun, S. Wang, H.M. Ang, M.O. Tadé, Q. Li, Chem. Eng. J. 162 (2010) 437–447.

[13] Y. Cao, T. He, L. Zhao, E. Wang, W. Yang, Y. Cao, J. Phys. Chem. C 113 (2009) 18121-18124.

[14] R.H. Sui, J.L. Young, C.P. Berlinguett, J. Mater. Chem. 20 (2010) 498-503.

[15] P.Wang, P.S. Yap, T.T. Lim, Appl. Catal. A: General 399 (2011) 252–261.

[16] C. Odetola, L. Trevani, E.B. Easton, J. Power Sources 294 (2015) 254-263.

[17] D. Gubán, I. Borbáth, Z. Pászti, I. E. Sajó, E. Drotár, M. Hegedűs, A. Tompos, Appl. Catal. B: Environmental 174 (2015) 455-470.

[18] S.H.S. Zein, A.R. Boccaccini, Ind. Eng. Chem. Res. 47 (2008) 6598–6606.

[19] N. Arconada, A. Duran, S. Suarez, R. Portela, J.M. Coronado, B. Sanchez, Y. Castro, Appl. Catal. B: Environmental 86 (2009) 1–7.

[20] S. Islam, N. Bidin, S. Riaz, R.A. Rahman, S. Naseem, F M. Marsin, Sens. Actuators B: Chemical 221 (2015) 993–1002.

[21] F. Schmit, L. Bois, R. Chiriac, F. Toche, F. Chassagneux, M. Besson, C. Descorme, L. Khrouz, J. Solid State Chem. 221 (2015) 291–301.

[22] W. Cui, L. Feng, C. Xu, S. Lu, F. Qiu, Catal. Commun. 5 (2004) 533–536.

[23] W.C. Lin, W.D. Yang, I.L. Huang, T.S. Wu, Z.J. Chung, Energy Fuels 23 (2009) 2192–2196.

[24] A.L. Linsebigler, G. Lu, J.T. Yates, Jr. Chem. Rev. 95 (1995) 735-758.

[25] J. Yang, D. Wang, H. Han, C. Li, Acc. Chem. Res, 46 (2013), 1900-1909 and the references cited herein.

[26] S. Trasatti, J. Electroanal. Chem. 39 (1972) 163–184.

[27] S. Shironita, K. Mori, T.Shimizu, T. Ohmichi, N. Mimura, H. Yamashita, Appl. Surf. Sci. 254 (2008) 7604–7607.

[28] B. Kraeutler, A.J. Bard, J. Am. Chem. Soc. 100 (1978) 4317–4318.

[29] Z. Jiang, W. Shangguan, Catal. Today 242 (2015) 372–380.

[30] S. Schafer, S.A. Wyrzgol, R. Caterino, A. Jentys, S.J. Schoell, M. Havecker, A. Knop-Gericke, J.A. Lercher, I.D. Sharp, M. Stutzmann, J. Am. Chem. Soc. 134 (2012) 12528–12535.

[31] M. Che, O. Clause, C. Marcilly, 4.1 Deposition of active component, in: G. Ertl, H. Knözinger, J. Weitkamp (Eds.), Preparation of Solid Catalysts, Wiley-VCH, Weinheim, 1999, pp. 315-371

[32] K. Maeda, K. Teramura, N. Saito, Y. Inoue, K. Domen, J. Catal. 243 (2006) 303–308.

[33] K. Majrik, E. Tálas, Z. Pászti, I. Sajó, J. Mihály, L. Korecz, E. Drotár, A. Tompos, Appl. Catal. A: General, 466 (2013), 169–178.

[34] Q. Gu, J. Long, H. Zhuang, C. Zhang, Y. Zhou, X. Wang, Phys, Chem. Chem. Phys, 16 (2014) 12521–12534.

[35] W. Zhao, M. Zhang, Z. Ai, Y. Yang, H. Xi, Q. Shi, X. Xu, H. Shi, J. Phys. Chem. C 118 (2014) 23117-23125.

[36] L. Zhang, Y. Li, Q. Zhang, H. Wang, Appl. Surf. Sci. 319 (2014) 21–28.

[37] B.S. Huang, F.Y. Chang, M.Y. Wey, Int. J. Hydr. Energy 35 (2010) 7699–7705.

[38] S. Song, Z. Sheng, Y. Liu, H. Wang, Z. Wu, J. Environmental Sci. 24 (2012) 1519–1524.

[39] B. Wang, C. Li, H. Cui, J. Zhang, J. Zhai, Q. Li, Chem. Eng J. 223 (2013) 592–603.

[40] J. Xing, Y.H. Li, Y. Wang, H.G. Yang, Int. J. Hydrogen Energy 39 (2014) 1237–1242.

[41] J.F. Moulder, W.F. Stickle, P.E. Sobol, K.D. Bomben, Handbook of X-Ray Photoelectron Spectroscopy, Perkin-Elmer Corp., Eden Prairie, Minnesota, USA, 1992.

[42] C.D. Wagner, A.V. Naumkin, A. Kraut-Vass, J.W. Allison, C.J. Powell, J.R. Rumble Jr, NIST X-ray Photoelectron Spectroscopy Database, Version 3.4, National Institute of Standards and Technology, Gaithersburg, MD 2003, http://srdata.nist.gov/xps/

[43] N. Fairley, www.casaxps.com/

[44] M. Mohai, Surf. Interface Anal. 36 (2004) 828-832.

[45] M. Mohai, "XPS MultiQuant: Multi-model X-ray photoelectron spectroscopy quantification program." Version 7.00.92 (2011), http://www.chemres.hu/aki/XMQpages/XMQhome.htm/

[46] Y. Jiang, J. Scott, R. Amal, Appl. Catal. B: Environmental 126 (2012) 290–297.

[47] Y. Jiang, R. Amal, Appl. Catal. B: Environmental 138–139 (2013) 260–267.

[48] A. Naldoni, M. D'Arienzo, M. Altomare, M. Marelli, R. Scotti, F. Morazzoni, E. Selli, V. Dal Santo, Appl. Catal. B: Environmental 130-131 (2013) 239–248.

[49] F. Lin Y. Zang, L. Wang, Y. Zhang, D. Wang, M. Yang J. Yang, B. Zhang, Z. Jiang, C. Li, Appl. Catal. B: Environmental 127 (2012) 363–370.

[50] J.A.R. van Veen, F.T.G. Veltmaat, G. Jonkers, J. Chem. Soc. Chem. Commun. (1985) 1656–1658.

[51] M.A. Henderson, Langmuir 12 (1996) 5093–5098.

[52] A.Y. Nosaka, T. Fujiwara, H. Yagi, H. Akutsu, Y. Nosaka, J. Phys. Chem. B 108 (2004) 9121–9125.

[53] A.Y. Nosaka, E. Kojima, T. Fujiwara, H. Yagi, H. Akutsu, Y. Nosaka, J. Phys. Chem. B 107 (2003) 12042–12044.

[54] A.Y. Nosaka, T. Fujiwara, H. Yagi, H. Akutsu, Y. Nosaka, Langmuir 19 (2003) 1935–1937.

[55] L.B. Xiong, J.L. Li, B. Yang, Y. Yu, Hindawi Publishing Corporation Journal of Nanomaterials, (2012) Article ID 831524, 13 pages doi:10.1155/2012/831524.

[56] B.C Gilbert, M.J Davies, D.M. Murphy, Special Periodical Reports, Electron Paramagnetic Resonance, Volume 21, RSC Publishing, 2008.

[57] J.L. Margitfalvi, I. Borbáth, K. Lázár, E. Tfirst, A. Szegedi, M. Hegedűs, S. Gőbölös, J. Catal. 203 (2001) 94–103.

[58] J.L. Margitfalvi, I. Borbáth, M. Hegedűs, Á. Szegedi, K. Lázár, S. Gőbölös, S. Kristyán, Catal. Today, 73 (2002) 343–353.

[59] R.B. Shalvoy, P.J. Reucrofty, J. Electron. Spectrosc. Relat. Phenom. 12 (1977) 351–356.

[60] D.R. Jennison, O. Dulub, W. Hebenstreit, U. Diebold, Surf. Sci. 492 (2001) L677–L687.

[61] Yu.I. Yermakov, B.N. Kuznetsov, V.A. Zakharov (Eds.) Catalysis by Supported complexes, Stud. Surf. Sci Cat. 8, Elsevier, Amsterdam, 1981, pp. 354–355.

[62] R. Bouwman, L.H. Toneman, A.A. Holscher, Surf. Sci. 35 (1973) 8–33.

[63] E. Merlen, P. Beccat, J. C. Bertolini, P. Delichčre, N. Zanier, B. Didillon, J. Catal. 159 (1996) 178–188.

Figure captions

Figure 1. Preparation way and denomination of the various Sn-Pt/TiO$_2$ catalysts

Figure 2. Raman spectra of TiO$_2$ samples with and without different type of cocatalyst.
a: SnOx-SG; b: SnOx-SG Pt Calc; c: no-Sn; d: SnOx-I; e: SnOx-I Pt Calc

Figure 3. Hydrogen production over sol-gel prepared TiO$_2$ samples. Sequence of cocatalyst introduction: Sn-first, Pt-second. Pt cocatalyst formation by high temperature H$_2$ treatment (Pt H2 red) and calcination (Pt Calc)

Figure 4. ^{1}H MAS NMR spectra of the different sol-gel prepared TiO$_2$ samples without evacuation a: no-Sn; b: SnOx-SG, c: SnOx-I; (a: 0.073 g, b: 0.079 g, c: 0.060 g)

Figure 5. Different types of surface OH groups of TiO$_2$ (based on Ref. [46**Hiba! A könyvjelző nem létezik.**])

Figure 6. ESR spectra of selected samples obtained from sol-gel TiO$_2$. (SnOx-I)
A: cocatalyst formation by high temperature hydrogen treatment a: Pt-free; b: SnOx-I Pt H2 red; c: recovered SnOx-I Pt H2 red;
B: cocatalyst formation by calcination, a: Pt-free; b: SnOx-I Pt Calc; c: recovered SnOx-I Pt Calc;

Figure 7. Dependence of hydrogen production on the relative signal intensity of vacancies in the recovered samples. ♦-Cocatalyst formation by calcination, □-cocatalyst formation by high temperature hydrogen treatment.

Figure 8. Diffuse reflectance UV-vis spectra of different TiO$_2$ samples.
A: platinum free TiO$_2$ samples, a: without tin (no-Sn), b: tin introduced by impregnation (SnOx-I); c: tin introduced by sol-gel method (SnOx-SG);
B: Pt cocatalyst formation by hydrogen treatment on SnO$_x$-TiO$_2$ (SnOx-SG), a: SnOx-SG; b: SnOx-SG Pt H2 red, c: recovered SnOx-SG Pt H2 red;
C: cocatalyst formation by calcination a: SnOx-SG; b: SnOx-SG Pt Calc, c: recovered SnOx-SG Pt Calc.

Figure 9. Oxidation state of platinum in the samples with cocatalyst formed by calcination

A: SnOx-I Pt Calc; B: SnOx-SG Pt Calc; C: no-Sn Pt Calc

Figure 10. Oxidation state of platinum in the samples with cocatalyst formed by high temperature hydrogen treatment

A: SnOx-I Pt H2 red; B: SnOx-SG Pt H2 red; C: no-Sn Pt H2 red

Figure 11. The effect of *in situ* H_2 treatment on the Sn 3d (A) and Sn MNN Auger (B) spectra of sample SnOx-I Pt H2 red. The reduction was performed at $T_{H2}= 200\ ^{o}C$ for t=60 min

Figure 12. Correlations between the hydrogen production and the surface atomic ratios. Data presented in this Figure are collected in Table S1 in the Supplementary Material)

Figure 13. A simplified scheme of the assumed transformations of the supported nanoparticles prepared by different cocatalyst formation